ORIGINAL PAPER

Rock Breakage and Tools Performance During Rock Processing by Multidiameter Combination Saw with Different Diameters

Jingguo Zhou[1,2,3] · Kaida Wang[1,2,3] · Jinsheng Zhang[1,2,3] · Heng Zhang[1,2,4] · Tianyu Cao[1,2,3] · Junwei Ju[1,2,3]

Abstract

To better understand the rock breakage mechanism and optimize tool performance during rock machining by multidiameter combination saw, the rock processing experiment using a multidiameter combination saw was carried out on the bridge saw to investigate the variation of load with diameter in the combination saw. Furthermore, in this study, the sawing forces, tools wear, and rock breakage in the processing rock were qualitatively analyzed and compared. The experimental investigations demonstrated that the maximum undeformed chip thickness, the load per diamond, and the load in the sawing arc zone all decrease with increasing diameters of the single saw in the combination saw. The sum of the vertical forces of the single saw is generally less than that of the combination saw under the same parameters because of the existence of the coupling effect between the single saws. Different failure mechanisms of particles in the worn segment of the tool with different diameters also operate in rock processing using a multidiameter combination saw. With increasing diameter of saw blade, the proportion of the whole and blunt diamond particles increases, and that of the macro-fractured and pulled-out crystals decreases. Moreover, the differences in the surface integrity are attributed to the variation in the maximum undeformed chip thickness on the saw blade with different diameters in the combination saw and the gully depth on the surface, and the surface roughness of rock decreases with increasing diameter of the single saw.

Highlights

- The experiments for rock processing by a multidiameter combination saw are designed to investigate the sawing performance of multidiameter combination circular saw with different diameters.
- Different failure mechanisms of particles in the worn segment of the tool with different diameters operate in rock processing using a multidiameter combination saw.
- The differences in the surface integrity are attributed to the variation in the maximum undeformed chip thickness on the saw blade with different diameters in the combination saw.
- Coupling effect between the single saws affects decomposition and generation of forces in the multidiameter saw.

✉ Jinsheng Zhang
zhangjs@sdu.edu.cn

✉ Heng Zhang
hengzhang@sdu.edu.cn

1 School of Mechanical Engineering, Shandong University, Jinan 250061, China

2 Key Laboratory of High-Efficiency and Clean Mechanical Manufacture (Ministry of Education), School of Mechanical Engineering, Shandong University, Jinan 250061, China

3 Research Institute for Intelligent Manufacturing, Shandong University, Rizhao 276800, China

4 Shenzhen Research Institute of Shandong University, Shenzhen 518057, China

List of Symbols

h_{max}	Maximum undeformed chip thickness (um)
Q_w	Material removal rate (mm²/s)
v_w	Feed speed (mm/s)
θ_g	Semi-included angle of the chip shapes of grain point, which was considered with a triangular section (rad)
a_p	Sawing depth (mm)
θ	Angle of sawing zone (rad)
d_s	Circular saw diameter (mm)
v_s	Linear velocity of circular saw (mm/s)
ω	Angular velocity of circular saw (rad/s)
$C_a = C\eta\lambda/l_s B$	The active grain density, which is defined as the number of active grits per unit area of the circumference surface
C	Number of effective abrasive particles on the surface of a single segment
η	Specific value, which is the proportion of the actual abrasive particles involved in sawing to the number of effective abrasive particles
$\lambda = l_s/l_s + l_w$	Specific value between the total length of diamond segments and the saw blade circumference
α	Angle of sawing arc zone (rad)
β	Angle of the position of the resultant force (rad)
l_c	Length of sawing arc zone (mm)
l_s	Length of segment (mm)
l_w	Length of slot (mm)
B	Width of the segment (mm)
f_t	The tangential load per diamond (N)
f_n	The normal load per diamond (N)
F_t	Sawing tangential force (N)
F_n	Sawing normal force (N)
F_z	Sawing vertical force (N)
F_y	Sawing horizontal force (N)
F_x	Sawing axial force (N)
i	Number of circulars saw $i = 1, 2, 3$

1 Introduction

Granite has been widely used in various fields and places due to its stable performance and superior characteristics. Nonetheless, high hardness and high wear resistance of granite make its efficient processing very difficult (Güneş Yılmaz 2011). At present, natural granite is mainly processed with diamond tools (Polini and Turchetta 2004a; Aydin et al.2013a and Zhang et al. 2016), and circular diamond saw is usually the main tool for granite processing (Gupta 2018; Celep and Aydin 2013). Good tool performances play an important role in the efficient processing of granite.

Many researchers studied the rock sawing process using a diamond tool to gain a thorough understanding of the rock breakage and improve tool performance. The research direction and main points of rock processing by diamond tools are systematically listed in Table 1. This study mainly focused on sawing force, tool wear, and rock breakage after processing. Furthermore, these three aspects are complementary and affect each other. The worn segments on the saw blade will increase the tangential force and normal force after the saw blade had been used for a long time, emphasizing that the sawing performance was affected by the wear of cutting tools (Xu et al. 2003). Turchetta et al. (2012) further investigated the cutting force of diamond tools under five different wear statuses of particles, indicating that the sawing forces calculated by equivalent chip thickness increase with increasing wear under five wear conditions. In the field of processing rock by frame saws, Sun et al. (2017) investigated the effects of cutting parameters and stone properties on the cutting force and pointed out that the feed speed and uniaxial compressive strength were the primary factors affecting the cutting force. Bayram and Kulaksiz (2021) evaluated the rock sawing performance of the diamond tool in terms of segment wear and established this as an important research method for analyzing the relationship between the advance rate and segment wear in frame saws. Besides, the effect of noise has also been used as one of the factors to analyze the performance of tools during rock processing (Karakurt et al. 2013a, b).

Many measurements and analysis methods are used in rock processing by diamond tools. Finite element technology is widely used in various fields, and rock processing is no exception. Wang et al. (2020b) established a two-dimensional (2D) rock model based on the hybrid finite-discrete element method, and zero thickness cohesive elements were inserted to simulate crack propagation in rock processing. The results showed that the tangential force slightly decreased, while the normal forces significantly increased with increasing abrasive angle. Furthermore, regression analysis and neural network analysis have also been used for establishing the predictive models in rock processing to analyze tool performance (Karakurt et al. 2013a, b; Aydin et al. 2015). In terms of wear and surface analysis, scanning electron microscopy has been widely used for wear observation and characterization. In addition, inductively coupled plasma (Inal et al. 2019) and a laser device (Ucun et al. 2013; Buyuksagis et al. 2020) were designed and applied in the wear detection of the circular saw blade. Irrespective of

Table 1 Related studies and main contents in rock processing by the diamond tool

Authors (Year)	Main contents
Luo (1996) and Tönshoff et al. (2002)	Their analysis indicated that the wear of diamond tool can be divided into two parts: the wear of metal bond and the wear of diamond, and the failure morphology of diamond can be classified into fresh, whole, micro-fractured, macro-fractured, blunt, and pulled-out diamond particles
Polini and Turchetta (2005)	A new wear test method for diamond tools was proposed, leading to comparable data for evaluating the wear of diamond tools
Pellegrin et al. (2009)	The effect of diamond particle shapes on wear was analyzed, the results indicated that the parameters of diamond particle shape, including the sharpness and convexity, are used to estimate the prediction of abrasive wear rate
Aydin et al.(2013b)	New methods for monitoring the wear of tool were discussed. Sawability evaluations for many types of rock can be performed quickly and without complex sawing tests
Karakurt et al. (2013a, b)	Granite cutting experiments were carried out. Force prediction models for rock properties and sawing parameters were established
Aydin et al. (2013c)	Surface roughness was investigated in rock sawing. The rock grain size was found as the dominant factor toward the main rock properties governing the surface roughness
Tumac (2015)	Schmidt hammer hardness values were used to assess the performance of large diameter circular saws
Turchetta et al. (2017)	Forces affected by pre-twisting and tensioning can optimize bead wear
Goktan and Gunes (2017)	The potential usability of Knoop micro-hardness for the assessment in the machining of granites was analyzed, recommending that the Knoop indentation technique may be used to investigate the wear performance of saw blade
Kansteiner and Biermann (2019)	The effect of diamond shapes on material removal was investigated. A diamond grain with a leading-edge was more conducive to material removal
Rajpurohit et al. (2020a)	The correlation between the Cerchar hardness index of granite rocks and the wear of diamond wire saw beads was discussed, and the regression models for the dataset were developed to obtain the statistical relationship between the rock hardness and diamond tool wear
Rajpurohit et al. (2020b)	Abundant models were constructed based on rock characteristics, considering the mineral composition, strength, hardness, and so on. Their results proved that rock characteristics significantly affect the cutting performance of tools
Soltani and Tayebi (2020)	A new type of metal binder that mainly contains copper was investigated, indicating that the wear resistance of this new type of metal binder was lower than the metal binders with high Co, Ni, and Fe contents
Bulut et al. (2021)	The sawing performance of the segments with the aluminum and silver was evaluated in terms of the wear characteristics

the research methods, the sawing force, tool wear, and rock breakage during rock processing directly or indirectly reflect the performance of diamond tools as indicated by the literature review. Therefore, the analysis of these three aspects is beneficial to thoroughly understand the rock processing process and improve its efficiency.

The machining stage of natural stone from rock blocks into plates is the most critical link to reduce costs and save resources. Recently, a new diamond tool with a multidiameter combination saw is often used for stone sawing in the process of industrial production. However, the literature reviews on circular saw blades indicate that the previous studies were only limited to the processing of a single circular saw blade, and the research on multidiameter combination saw is rarely reported. In particular, there is a

clear lack of the research on the relationship between the sawing force, tool wear, and rock breakage during the rock processing by the multidiameter combination saw. Zhang et al. (2016, 2019) reported the processing of granite by frame saws, not involving combination saws. Zhou et al. (2021) discussed the wear of segments on the combination saw, explaining the factors producing wear differences between the large and small saw blades. The disadvantage is that there is no actual sawing experiment to analyze the relationship between the force and the diameter of the saw blade. Yurdakul (2015) analyzed the effect of cutting parameters and cutting mode on power consumption by obtaining the data from the multi-blade block cutter without involving multidiameter combination saws. To design the combination saws more reasonably and improve the

rock breakage efficiency, it is necessary to investigate the tool performance during rock processing by the combination diamond circular saw.

To enhance the rock breakage efficiency, in this study, the sawing performance of a multidiameter combination saw, including sawing force, tool wear, and the surface of the processed rock was investigated. The relationship between the force of saw blades with different diameters, segment's wear, and the surface of the processed rock were analyzed and compared. In particular, a sawing experiment of granite by multidiameter combination saw was designed and carried out to verify the load model of combination saw, contributing to the design of a combination saw reducing wear nonuniformity of segments.

## 2 The Combination Saw Comprising Saw Blades of Different Diameters

2.1 The Structure Principle of Combination Saw

Multi-blade combination saw machine, also called as multi-blade block cutter, consists of multiple circular saw blades installed on the same spindle. The single saws are separated from each other by flanges of a certain thickness, forming the thickness of the sawn slabs. Diamond segments are usually layered, including soft metal matrix and stiff metal matrix. Rugged sawing trails are generated on the stone surface due to the special structure of segments. Multi-blade

combination saws are generally divided into three types: single diameter combined saw, consisting of saw blades with only one diameter; double diameter combination saw, consisting of saw blades with two diameters, and multidiameter combination saw, consisting of saw blades with different diameters. As a type of combination saw, the multidiameter combination saw is widely used in the sawing of rock blocks mainly to cut the rock blocks into rough slabs. A schematic diagram of rock sawing by combination saw is displayed in Fig. 1a and b. Sawing granite with a multidiameter combination saw is a clean technology for stone processing (Bai et al. 2020). Because of the support of the flange, the thinned saw blade will not suffer from the drastic lateral oscillation, and the thickness of the saw blade can be reduced to 2.5 mm. Compared with traditional circular saws, the processing technology of rock blocks with ultrathin multidiameter combination saw improves the cutting efficiency, reduces the width of the saw kerf, increases the plate output, indirectly saves energy, and reduces emission.

2.2 Theoretical Analysis of Forces for Combination Saw

The maximum undeformed chip thickness is a crucial variable in evaluating the cutting performance of diamond tools, as reported by Macerol et al. (2020). The maximum undeformed chip thickness, the load per particle, and the forces in the sawing arc zone in the combination saw are related to the saw diameter as follows (Zhou et al. 2021).
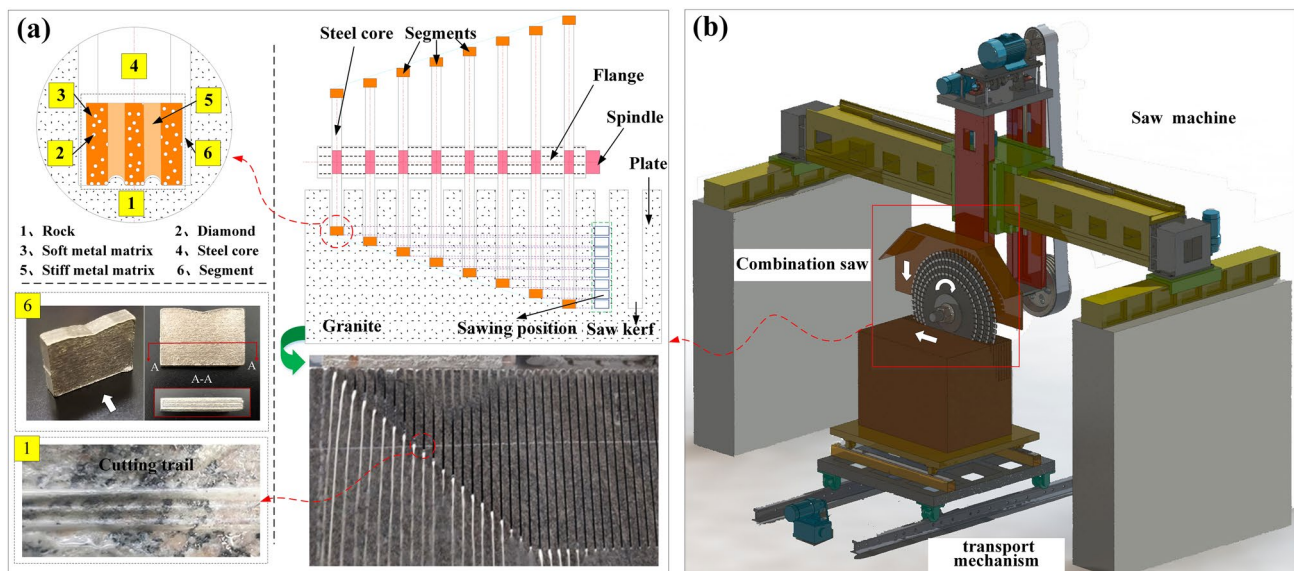
Fig. 1 Illustration of the multidiameter combination saw. **a** Schematic diagram of rock sawing by combination saw, and **b** combination saw machine

$$
\begin{cases}
h_{\max i} = \left[\frac{6\pi B v_w \sqrt{a_p}}{C\eta a\omega \tan\theta_g} \left(\frac{1}{d_{si}}\right)^{\frac{3}{2}} \right]^{1/2} \\[2mm]
f_{ti} = m_1 \left(\frac{6\pi B v_w \sqrt{a_p}}{C\eta a\omega \tan\theta_g} \left(\frac{1}{d_{si}}\right)^{\frac{3}{2}} \right)^{\frac{n_1}{2}} \\[2mm]
F_{ti} = \left[\left(\frac{6B v_w}{\omega \tan\theta_g}\right)^{\frac{n_1}{2}} m_1 (a_p)^{\frac{1}{2}+\frac{n_1}{4}} \right] \times \left(\frac{aC\eta}{\pi}\right)^{1-\frac{n_1}{2}} \times (d_{si})^{\frac{1}{4}(2-3n_1)}
\end{cases}, \tag{1}
$$

$$
\begin{cases}
h_{\max i} = \left[\frac{6\pi B v_w \sqrt{a_p}}{C\eta a\omega \tan\theta_g} \left(\frac{1}{d_{si}}\right)^{\frac{3}{2}} \right]^{1/2} \\[2mm]
f_{ni} = m_2 \left(\frac{6\pi B v_w \sqrt{a_p}}{C\eta a\omega \tan\theta_g} \left(\frac{1}{d_{si}}\right)^{\frac{3}{2}} \right)^{\frac{n_2}{2}} \\[2mm]
F_{ni} = \left[\left(\frac{6B v_w}{\omega \tan\theta_g}\right)^{\frac{n_2}{2}} m_2 (a_p)^{\frac{1}{2}+\frac{n_2}{4}} \right] \times \left(\frac{aC\eta}{\pi}\right)^{1-\frac{n_2}{2}} \times (d_{si})^{\frac{1}{4}(2-3n_2)}
\end{cases}, \tag{2}
$$

where m_1, m_2, n_1, and n_2 are constants, and $n_2 \in (1,2)$ in the rock sawing (Huang et al. (2017)). The maximum undeformed chip thickness, the load of per diamond, and the forces in the sawing arc zone are inversely proportional to the diameters of the saw blade according to Eqs. (1) and (2).

It is assumed that the load of the combination saw system can be expressed as the superposition of the load of the single saw system, as depicted in Fig. 2a, b and c. Considering the coupling effect of a single saw in the rock processing by combination saw, the constants (k_1, k_2) were introduced. Therefore, the horizontal force (F_y) and vertical force (F_z) of the combination saw can be written as:

$$
F_y = k_1 \sum_{i=0}^{s} F_{yi}, \tag{3}
$$
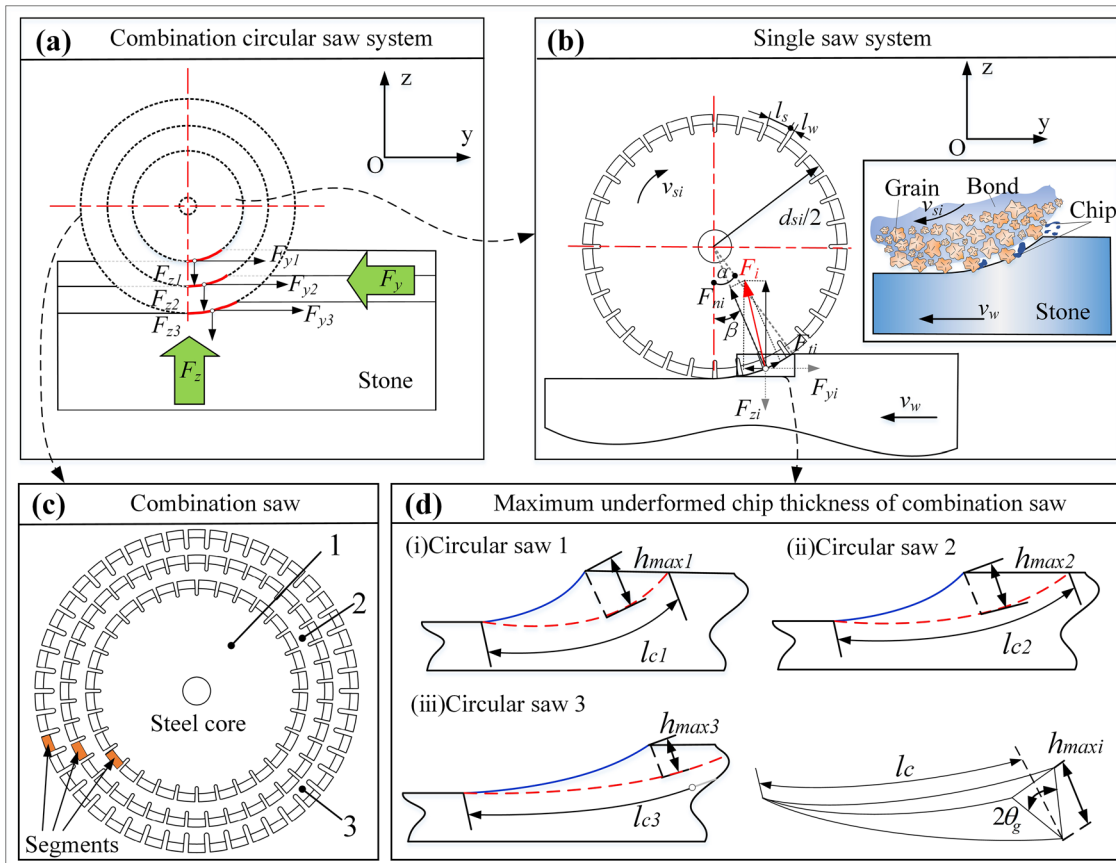
Fig. 2 The analysis of sawing force in combination circular saw. **a** Force analysis of a combination circular saw system, **b** force analysis of a single saw system, **c** number of combination saws, and **d** the maximum undeformed chip thickness of the particle in the saw blade of different diameters

$$F_z = k_2 \sum_{i=0}^{s} F_{zi}. \tag{4}$$

Moreover, the load of the single saw system is shown in Fig. 2b and can be expressed as

$$\begin{aligned} F_{yi} &= F_{ni} \sin(\beta_i) - F_{ti} \cos(\beta_i) \\ F_{zi} &= F_{ni} \cos(\beta_i) + F_{ti} \sin(\beta_i) \end{aligned}. \tag{5}$$

Generally, $\beta_i = k\alpha_i$, k is a constant and greater than zero, $\alpha_i = \cos^{-1}(1 - 2a_p/d_{si})$.

The effect of cosine function on F_{yi} and F_{zi} is dominated in rock sawing by the combination saw because of the small angle of β_i in the actual rock sawing, and thus the qualitative relationship between F_{yi} and F_{zi} can be mainly affected by the tangential force (F_{ti}) and normal force (F_{ni}). Therefore, the relationship between the F_{ti} and the F_{ni} with the variation of diameter can be reflected from the analysis of the horizontal force (F_{yi}) and vertical force (F_{zi}).

A negative correlation between the maximum unde-formed chip thickness and the diameter of the saw blade is expressed by Eqs. (1) and (2), indicating that the chip thickness decreases gradually under the same material removal rate ($Q_w = a_p v_w$), i.e., $h_{max\,1} > h_{max\,2} > h_{max\,3}$. With the variation of diameter of a single saw in the combination saw, the chip shape generated by diamond particles was transformed from short and thick type to thin and long type, as shown in Fig. 2d. The cutting conditions of the circular saw with the same rotating speed and different diameters in the combination saw system are similar to that of the single saw with the same diameter and different rotating speeds, which is essentially the variation of line velocity of the segment.

3 Materials and Methods

3.1 Experimental Materials

The experiments were conducted using a bridge saw machine. The saw machine was installed with a multidiameter combination saw. In the tests, the v_w was in the range 15–45 mm/s, the a_p was in the range 2–10 mm, and the rotating speed of the machine spindle was maintained at 1860 rpm approximately. A multidiameter combination saw comprising saw blades with three different diameters was chosen as the experiment tools. The saw blades consist of two parts: one part was of steel core made of 75Cr1 alloy steel, another part was layered diamond segments where the composition of the metal binder is the iron base, and both the parts were connected by high-frequency welding technology. The description of the diamond saw blades and segments used in the experiment are listed in Table 2. The experimental samples were Bai ma granite with the dimensions of 200 mm (length) × 100 mm (width) × 180 mm (height). The physical–mechanical properties of rock blocks are as follows: compressive strength, 112 Mpa; bending strength, 8.9 Mpa; water absorption, 0.37%, and density, 2.69 g/cm^3.

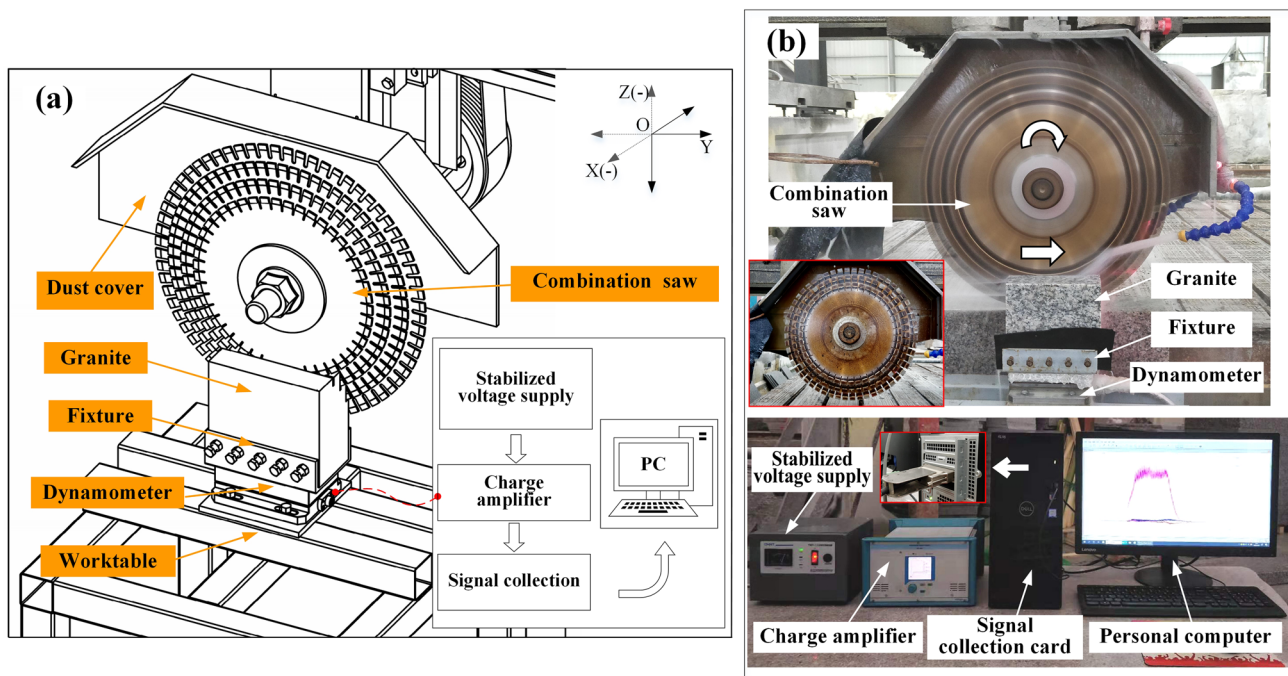## 3.2 Sawing Tests

3.2.1 Sawing Force Measurement

Figure 3a illustrates the schematic diagram of force measurement. The sawing forces were captured using a Kistler piezoelectric dynamometer (9257B) with high rigidity, high natural frequency, and high resolution. The dynamometer was fixed on the worktable by M8 bolts, many heavy rock blocks were placed on the workbench to reduce interference from unnecessary vibration, and the granite samples were mounted on the dynamometer by the fixture. During the sawing process, the force signals in three directions (F_x, F_y, and F_z) were recorded by the sensor in the dynamometer and transmitted to the charge amplifier through a data cable. The charge signals processed by the charge amplifier were transmitted to signal collection, sampled, processed, and displayed with a computer. Figure 3b shows the image of the experiment.

### 3.2.2 Tests of Worn Segments and Rock Surface

The worn segments with an equal number of intervals were selected for observation, as shown in Fig. 4. A total of 24

Table 2 Description of the diamond saw blades and segments used in the experiment

Number	External diameter (mm)	Inner diameter (mm)	Thickness (mm)	Teeth's number	Slot sizes (mm)		Diamond segments		
					Width	Depth	Size (mm)	Particle size	Bond
1	390	50	3	44	3	18	22 (length) × 4.3 (width) × 15 (height)	40/50 (mesh)	Iron base
2	460			50	5				
3	530			56	5				

Fig. 3 Experimental setup of the multidiameter combination saw sawing test. **a** Schematic diagram of force measurement, and **b** scene picture during the field test
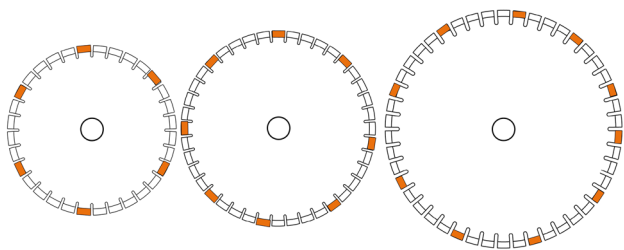
Fig.4 Sampling diagram of worn segments

worn segments were observed in the tests, and the number of segments observed in each saw blade was 6, 8, 10. The failure modes of diamond particles in the worn segments were counted and analyzed using an optical microscope. The failure mechanism of diamonds on the worn segments of the saw blade with different diameters was investigated by scanning electron microscopy (SEM). Furthermore, the sawing trails of rock surface after sawing were investigated by laser confocal microscopy.

The flowchart for this study is presented in Fig. 5. A sawing experiment for the rock sawing by the multidiameter combination saw was designed to verify the change in the force with diameter in the combination saw model established in Theoretical Analysis of Forces for Combination

Saw. Differences in the worn segments between single saws of different diameters were analyzed by multi-diameter saws. Finally, the surface roughness and rock breakage of rocks sawn by the multidiameter combination saw were investigated based on the above finding.

4 Results and Discussion

4.1 Sawing Force Characteristics

4.1.1 Waveform Analysis of Sawing Force

Figure 6 shows a typical waveform of the sawing force of the combination saw, reflecting the variation in sawing processing. Figure 6a, b shows the filtered sawing force and the original sawing force, respectively, indicating that the sawing processing consists of five stages: sawing entry stage, initial sawing stage, steady sawing stage, late sawing stage, and sawing completion stage. The division of stages during the rock sawing by combination saw and the positional relationship between the combination saw and rock processed are displayed in Fig. 7.

The sawing entry stage (Fig. 7a), i.e., the phase where the combination saw starts the feed motion until the

Fig. 5 The flowchart for this study
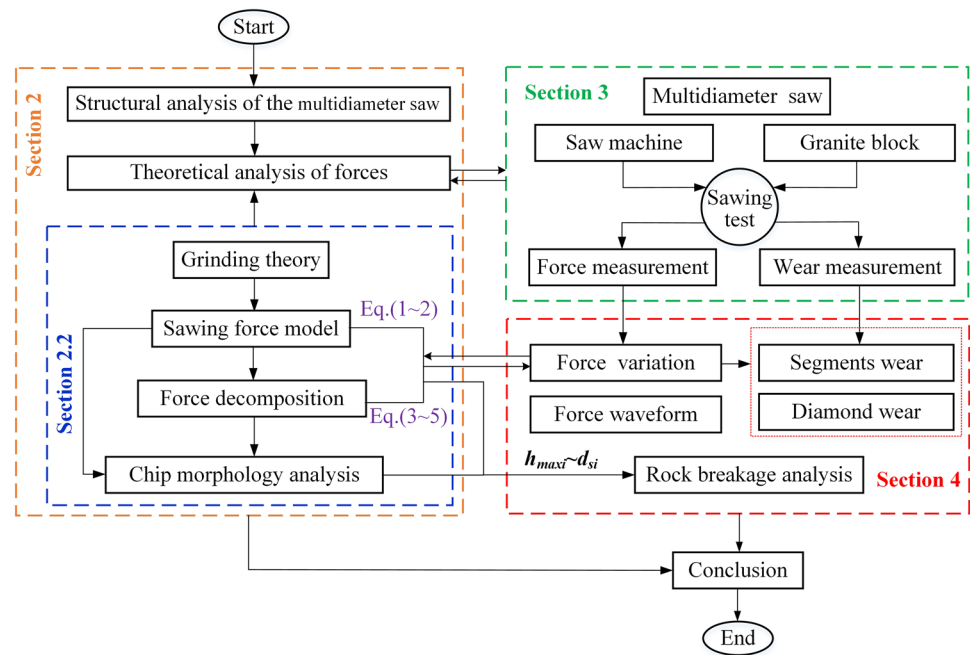
sawing entry points contact the rock was considered to be a stage in which each saw blade in the combination saw enters the saw kerf one by one. The horizontal forces (F_y) and vertical forces (F_z) remain zero in this stage, and transverse vibration generated by the high-speed rotation of the saw blade scratches between the saw blade and the rock processed, generating slight axial force F_x, as shown in Fig. 6b. The initial sawing stage (Fig. 7b) is the phase where the sawing entry points touches the rock until the length of the sawing arc zone of each saw blade reaches a definite value under a fixed sawing depth. At this stage, each saw blade cuts into the rock gradually, the length of the sawing arc zone of each saw blade increases, and the sawing force in all the directions (F_x, F_y, and F_z) increases. Among them, the vertical force (F_z) changed most prominently, as shown in Fig. 6b. Increased contact length in rock sawing linearly increases the sawing force. The steady sawing stage (Fig. 7c) is from the phase where the length of the sawing arc zone of each saw blade reaches a definite value to the length of the sawing arc zone of each saw blade begins to decrease. The length of the sawing arc zone of each saw blade remains constant in this stage, and the sawing force of the combination saw fluctuates up and down around a certain value, with periodic changes in

the waveform, as shown in Fig. 6b. The late sawing stage (Fig. 7d) starts from the stage where the length of the sawing arc zone of each saw blade begins to decrease so that all the saw blade does not contact the rock, as illustrated in Fig. 6b. Reducing the arc length of each saw blade in rock sawing decreases the sawing force linearly. The sawing completion stage (Fig. 7e) starts from the phase where all the saw blade does not contact the rock to the end of the feed motion of the combination saw, and this was considered to be a stage in which the waveform of the sawing force at this stage is similar to that of the sawing entry stage. Slight axial force (F_x) was generated by the transverse vibration caused by the high-speed rotation, as shown in Fig. 6b.

Figure 6a, b clearly shows that the sawing force (including vertical force F_z, horizontal force F_y, and axial force F_x) all first present an increasing trend, then remains unchanged, and finally decreases during the whole sawing cycle. The cutting force mainly originated from the reaction force generated by the deformation and fracture of the rock material, producing the friction force between the tool and the rock surface and the chip during the cutting process of rock materials (Wang et al. 2020a). The reaction force was directly dependent on the material removal volume in the
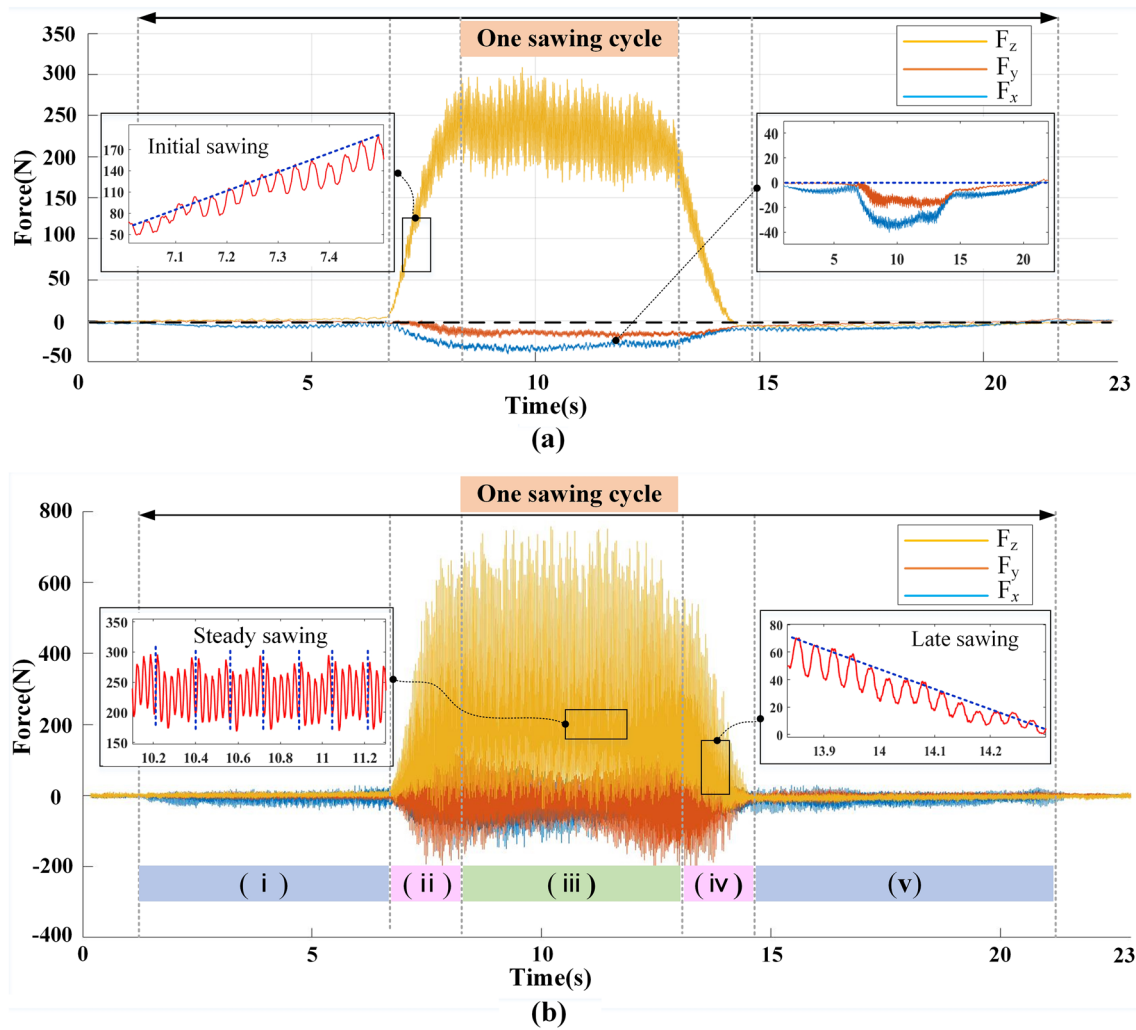
Fig. 6 The waveform analysis of the sawing force of combination saw (the sawing parameters are the sawing parameters are $n = 1860$ rpm, $a_p = 4$ mm, $v_w = 30$ mm/s), **a** filtered sawing force, and **b** original

sawing force: i—sawing entry stage, ii—initial sawing stage, iii—steady sawing stage, iv—late sawing stage, and v—sawing completion stage

rock sawing. The evolution of the above-mentioned cutting process eventually changes the material removal volume and the contact area, resulting in the variability of forces.

4.1.2 The Comparison and Analysis of Sawing Forces

The sawing forces of the single saw and the combination saw were measured under different sawing parameters, and the experimental sawing vertical forces are listed in Table 3. The filtering processing of force signals was completed by

Dynoware software, and the net increment in the sawing force during the sawing process was taken as the research object (the difference between the steady sawing stage and non-contact stage is referred to as the net increment). When the sawing depth is small, the volatile ups and downs of horizontal force are not obvious. Only vertical sawing forces are displayed for comparative and descriptive analysis owing to their clear and accurate reflection of the saw force's variation. The comparative analysis of the sawing force is as follows.

Fig. 7 Division of sawing stages of combination saw. **a** Sawing entry stage, **b** initial sawing stage, **c** steady sawing stage, **d** late sawing stage, and **e** sawing completion stage
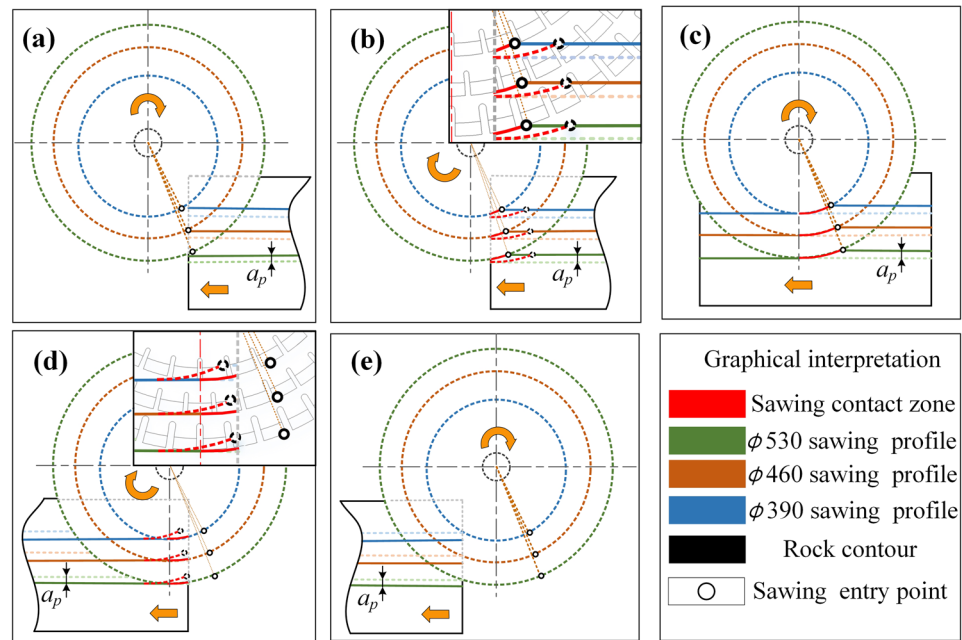
4.1.2.1 The Sawing Forces of the Single Saw and Combination Saw

The variation trend of the sawing forces of the single saw and the combination saw with sawing parameters is depicted in Fig. 8. The vertical sawing forces increase with increasing sawing depth and feed speed, which increase linearly, taking 30 mm/s as an example, when increasing the sawing depth from 2 to 10 mm. The vertical forces generated by φ390 circular saw, φ460 circular saw, and φ530 circular saw changed from 61.2 to 198 N, from 55.8 to 176 N, and from 21.3 to 85 N, respectively, and the vertical force of combination saw changed from 116.7 to 512 N, mainly attributing to the increase in the volume of material removed by diamond particles during increasing sawing depth, which increases the reaction force generated by the brittle fracture of rock. Thus, the variation rule of the vertical force following the sawing parameter is shown in Fig. 8. A similar conclusion, as reported by Turchetta and Sorrentino (2019), was obtained, indicating that the cutting force is directly proportional to feed per revolution and inversely proportional to the cutting speed raising in high-speed machining of granite.

4.1.2.2 The Relationship of Sawing Forces Between Single Saw and Combination Saw

The force variations of different tools with different sawing depths at different feed speeds (15, 30, and 45 mm/s) are shown in Fig. 9. Different colored areas represent the magnitude of vertical force, indicating that the color area gradually decreases with increasing diameter. This observation indicates that the sawing force between the single saw of the combination saw gradually decreases. Moreover, the sum of the vertical force of the single saw is generally less than that of the combination saw under the same sawing parameters. A selection of representative results for the comparisons of force at different cutting depths is shown in Fig. 9c. When choosing 4 mm of the sawing depth, the vertical force of single saw for φ390, φ460, and φ530 is 176 N, 162.2 N, 81.2 N, respectively, with a sum of 419.4 N. Noteworthy, the vertical force of combination saw is 452 N and is greater than the sum of the vertical force of three diameter saw blade. The same phenomenon was also observed for other cutting parameters, mainly attributed to the different chip thickness of particles in the segments, changing the force between the saw blades with different diameters.

The load model of the combination saw was demonstrated by the above phenomenon, concluding that the sawing force in the sawing arc zone decreases with increasing diameter. It is worth mentioning that the coupling effect between the sub-saws with different diameters during the rock sawing generates a series of additional forces, such as the larger radial excitation force, friction force of saw–plate–saw, and the impact force of the coolant mixed with debris, leading to the fact that the superimposed sawing force of single saw is generally less than the force of combination saw. This also indicates that the constant k_2 is greater than 1.

Table 3 The experimental vertical sawing force (N), $n = 1860$ rpm

Tools	v_w(mm/s)	a_p(mm)				
		2	4	6	8	10
φ390	15	55.5	75.0	87.0	102.0	151.8
	30	61.2	103.0	142.0	175.0	198.0
	45	75.0	145.0	176.0	227.0	259.1
φ460	15	31.2	52.8	73.0	90.0	112.0
	30	55.8	76.0	117.0	141.0	176.0
	45	64.0	111.0	162.2	189.0	239.0
φ530	15	20.3	23.3	44.5	50.0	69.0
	30	21.3	33.4	52.2	68.0	85.0
	45	31.9	59.0	81.2	111.0	137.0
Combination saw	15	76.5	160.0	151.0	395.0	430.0
	30	116.7	231.0	324.8	459.0	512.0
	45	205.8	397.0	452.0	605.9	670.6

4.2 Wear of the Segment

4.2.1 Wear Analysis of Diamond Particles

The surface morphology of the worn segments was observed by using a field emission high-temperature scanning electron microscope (JSM-7800F). The worn segments of diamond particles on the combination saw shows six different wear states (Zhang et al. 2019; Polini and Turchetta 2004b): (a) fresh diamonds (the cutting edge of the abrasive is exposed from the metal matrix slightly), (b) whole diamonds (perfect particles without damage and crack on the surface), (c) blunt diamonds (cutting edge is worn flat, and smooth surface is displayed), (d) micro-fractured diamonds (the surface of the whole diamond particles is slightly cracked or broken), (e) macro-fractured diamonds (micro-fractured grains further damage, diamond crystals crystal collapses and the surface is broken obviously), and (f) pulled-out diamonds (crystals exhibit a pit on worn matrix surface). Figure 10 shows different wear states of diamond particles on the combination saw.

The surface images of the worn segment obtained by the optical microscope were processed, where four to five images were stitched together to form a complete segment image, and different colors represent the different wear states of crystals (Fig. 11). The failure proportion of particles on the single saw with different diameters in the combination saw was obtained by data statistics. Figure 12 represents the failure proportions of the worn diamonds in the segments used by different diameter saws. With increasing diameters of the single saw, the proportion of the fresh, whole, and blunt diamond particles increases, and that of the micro-fractured, macro-fractured, and pulled-out crystals

decreases, indicating that the diamond particles gradually transform from abnormal failure to normal cutting.

The higher proportion of the micro-fractured, macro-fractured, and pulled-out crystals is shown in the worn segment of φ390 saw blade, accounting for 34.3%, 14.6%, and 17.2%, respectively, and the total proportions are as high as 66.1%. The proportion of the pulled-out diamonds dominates. In contrast, the worn segments do not show larger proportion of fresh, whole, and blunt diamonds (14.6%, 11.6%, and 7.7%, respectively). The inferior removal ability of diamond particles and widespread abnormal failure of grains are observed from the above phenomenon. In contrast to the former, traces of pulled-out grains in the matrix (21%) decreased significantly in the worn segment on the φ460 saw blade. Abrasive particles with cutting potential, such as whole, fresh and blunt diamond crystals (with the proportion of 19.7%, 16.6%, and 14%, respectively), display an upward trend, indicating enhanced material removal ability of diamond particles. The φ530 saw blade shows further growth for the proportions of the fresh, whole, and blunt diamond particles (16.9%, 21.1%, and 15.1%, respectively); however, it shows continued decline for the proportions of micro-fractured, macro-fractured, and pulled-out diamond particles (13%, 14.1%, and 19.8%, respectively). The largest proportion was observed for the whole grains rather than the pulled-out grains. In all of those phenomena, the diamond particles gradually transform from abnormal failure to normal cutting with increasing tool's diameter in the combination saw. In contrast to the wear mechanism reported in rock processing by the single saw (Güneş Yılmaz 2011; Aydin et al. 2013b), different failure mechanisms operate for particles in the worn segment of the tool with different diameters
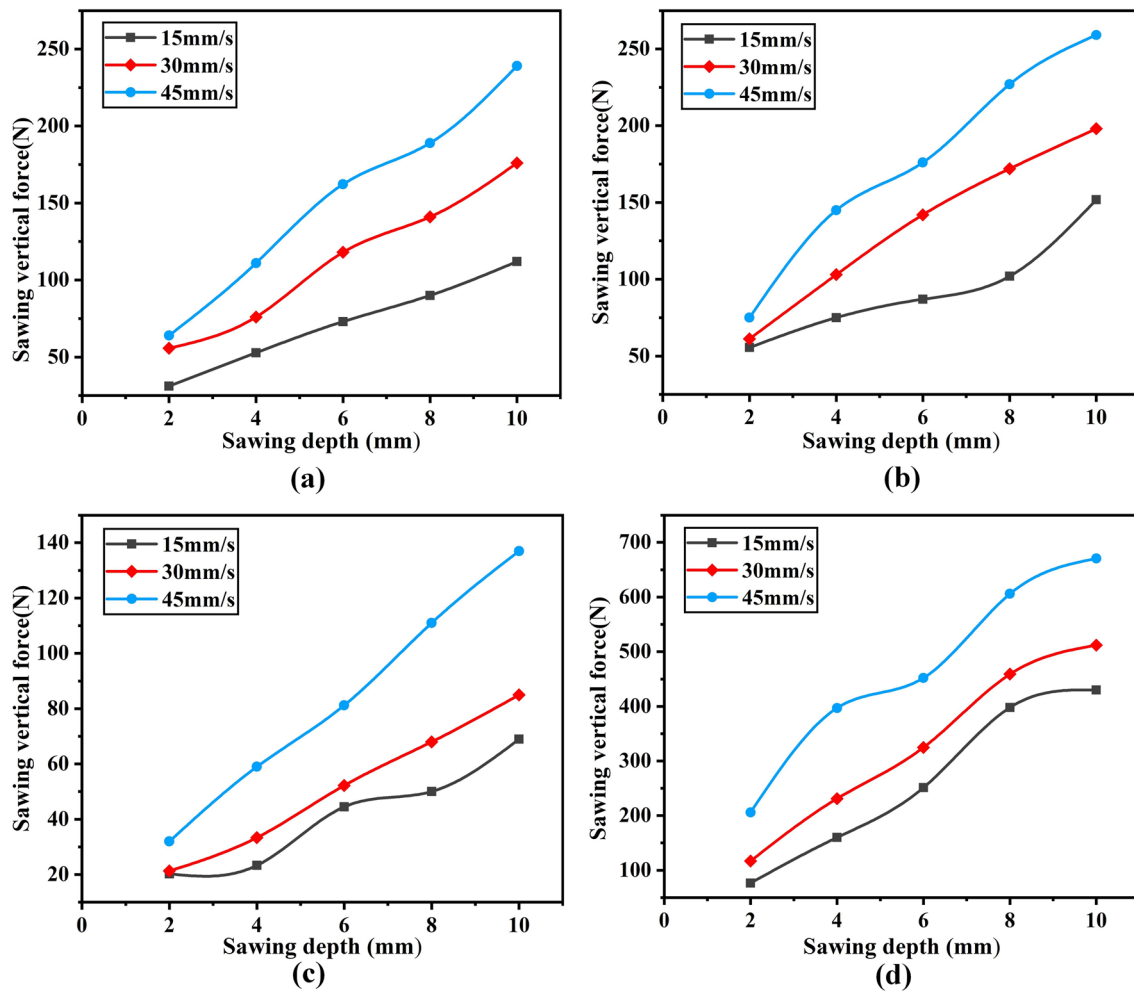
Fig. 8 The sawing forces of single saw and combination saw vary with sawing parameters, **a** φ390 circular saw, **b** φ460 circular saw, **c** φ530 circular saw, and **d** combination circular saw

in rock processing using a multidiameter combination saw. Notably, the failure proportion of diamonds varies with the diameter of the single saw.

Equations (1) and (2) show that with the increase of diameters of the single saw in the combination saw, the maximum undeformed chip thickness, the load per diamond, and the load in the sawing arc zone all decrease. The diameters of the single saw gradually increase in the combination saw. In cases of the φ390 saw blade, bearing larger impact force for the particles due to the large load in the sawing arc zone, there is an increase in the shear force borne by the particles in the sawing process than the retention capacity between the crystals and the metal binder. The following two wear states, including

fresh—macro-fractured—pulled-out or fresh—whole—pulled-out, will be dominated, leading to the loss of abrasive particles with cutting potential and the waste of diamond particles and the reduction of the material removal ability of the circular saw blade. With increasing diameters, the load on the diamond particles decreases gradually, and the diamond particles tend to normalization cutting.

4.2.2 The Surface Morphologies of Worn Segments

Figure 13 depicts the SEM images of the worn surfaces of the segments in the saw blade with different diameters taken using a scanning electron microscope. Figure 13a
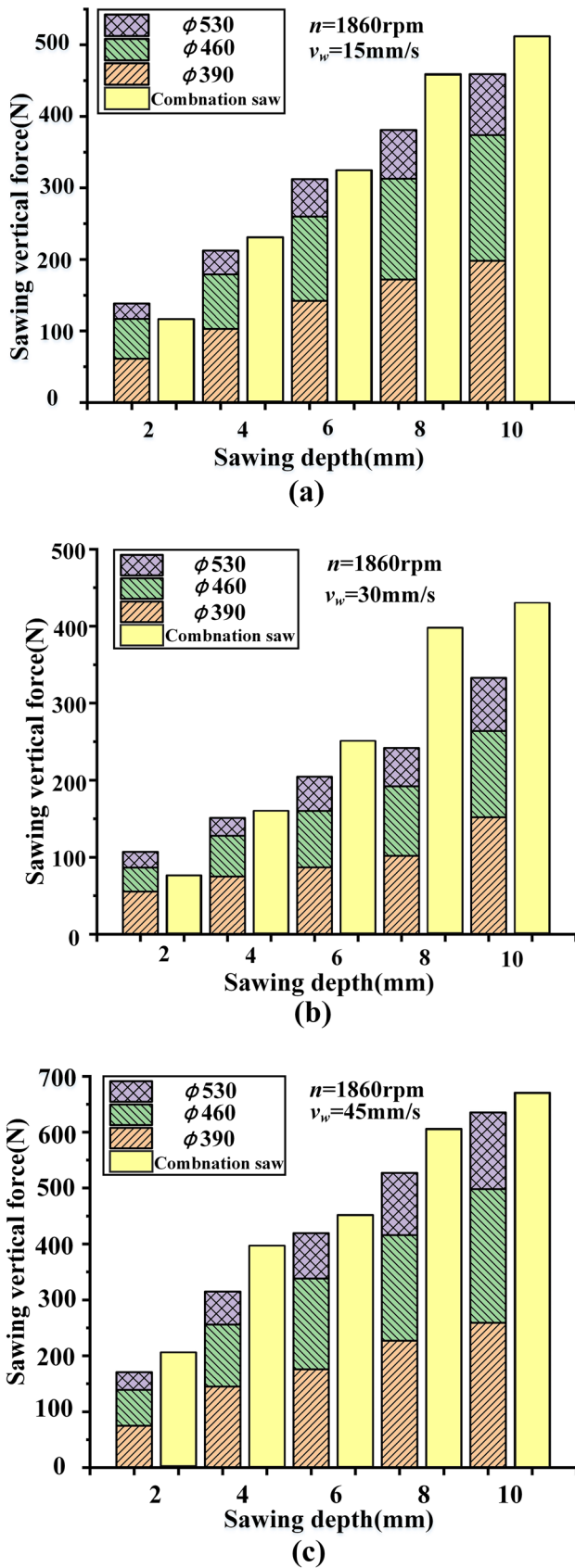
Fig. 9 The saw forces at different sawing depths and feed speed, **a** 15 mm/s, **b** 30 mm/s, and **c** 45 mm/s

indicates that the pulled-out diamonds dominate in the segment used by φ390 saw blade, and cracks occurred at the interface between the metal binder and crystals, peeling the particles easily. In contrast to the φ390 saw blade, the saw blade with larger diameters, i.e., φ460 and φ530 saw blades, the whole diamond particles dominate. The interface surface between the metal binder and crystals is tightly connected, as displayed in Fig. 13b and c. The diamond is not easy to fall off and has a better cutting ability. This is consistent with the wear analysis of diamond particles. This study shows some guidance for the design of the combination saw. The segments with the grains of different qualities or the segments with the metal binder with strong retention capacity adopted to the different saw blades may be beneficial to reducing the failure of the diamond.

4.2.3 The Analysis of Rock Breakage

The diamond segments used in this experiment are a layered cuboid, made of a soft metal matrix and stiff metal matrix by the hot pressing sintering process. Rugged sawing trails were generated on the stone surface after the rock processing due to different wear rates between the soft and stiff metal matrices. The valley and top parts correspond to the cutting area of diamond particles and the friction area of the soft metal matrix, respectively, as displayed in Fig. 14.

Stone mineral constituents were removed by abrasive grits to create uneven surfaces, which can reflect the removal mechanism of materials and the chip thickness of particles to a certain extent. The sawing trails of the rock were observed to acquire the surface topography and roughness Ra in the valley part by laser confocal microscopy (Fig. 15).

The surface topography and roughness of processed granite were compared, indicating different mechanisms of rock breakage operating in the rock processed with the saw blades of different diameters, as illustrated in Fig. 15a, b, c. The material removal mechanisms for diamonds cut by various saw blades are essentially similar, and the dominant removal mechanism of rock is a brittle fracture. With increasing diameter of the single saw, the gully depth on the surface of the processed rock decreases, and the rock surface tends to flatten out. The surface roughness of granite processed by the segment on the saw blade of different diameters is shown in Fig. 15d, indicating that the surface roughness of rock diminishes along with increasing diameter of the saw blade. Meanwhile, the chipping craters, gullies, and fractures on the rock surface were found as the main characteristics, similar to the studies in the literature (Aydin et al. 2013c). The differences in the surface integrity are attributable to the variation in the chip thickness per abrasive in the combination saw. Equations (1) and (2) show that a larger diameter of the saw blade generates a larger linear velocity of the segment, causing a smaller maximum undeformed chip
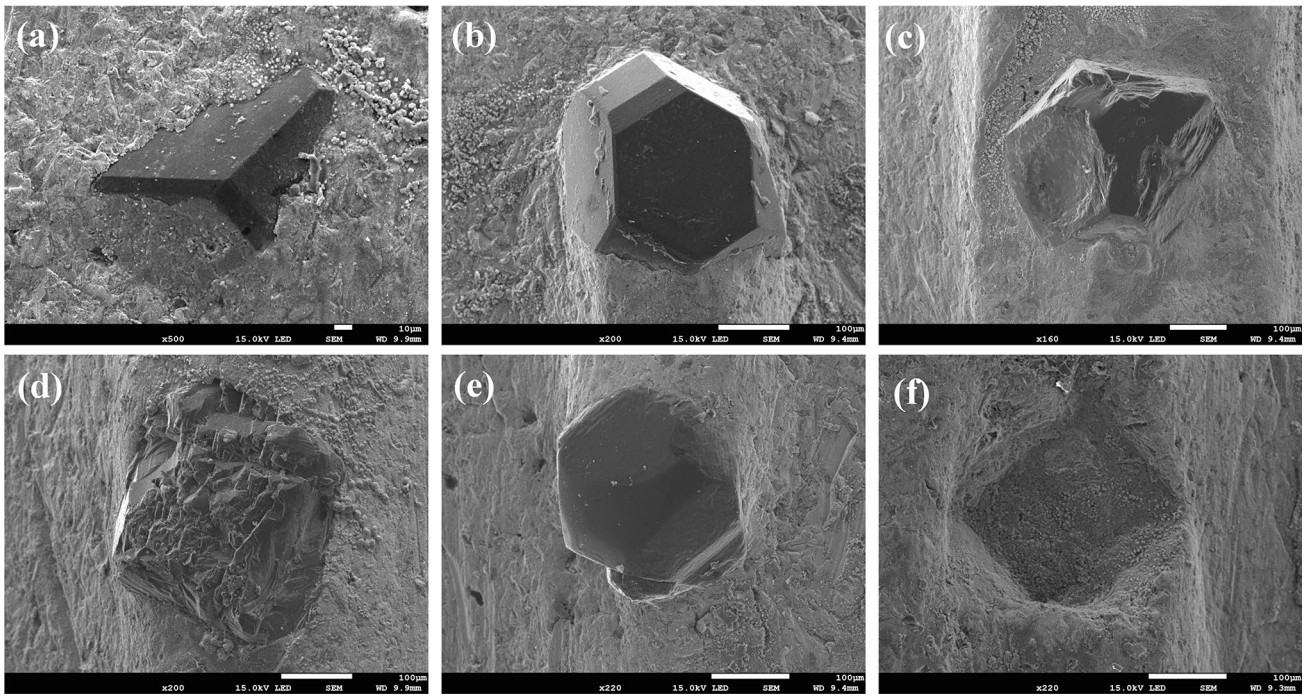
Fig. 10 Different wear states of diamond particles on combination saw, **a** fresh, **b** whole, **c** micro-fractured, **d** macro-fractured, **e** blunt, and **f** pulled-out crystals
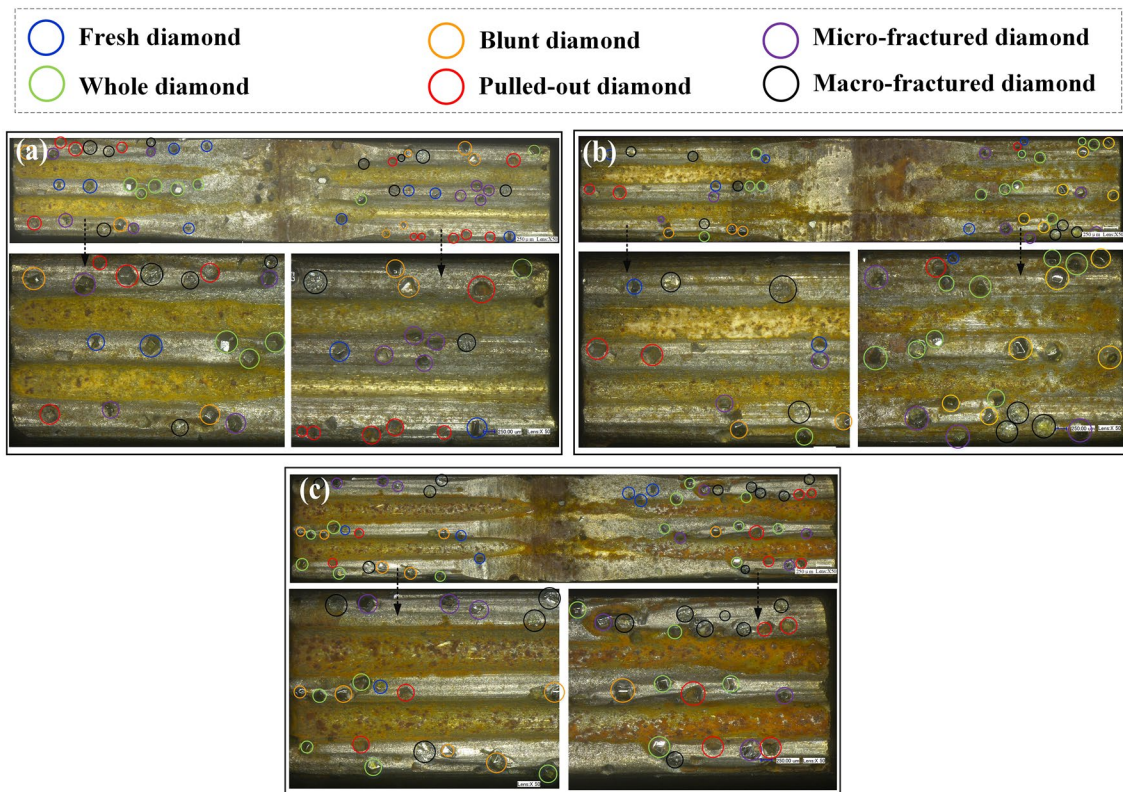
Fig. 11 Diamond particle statistics with the optical microscope, **a** φ390, **b** φ460, and **c** φ530
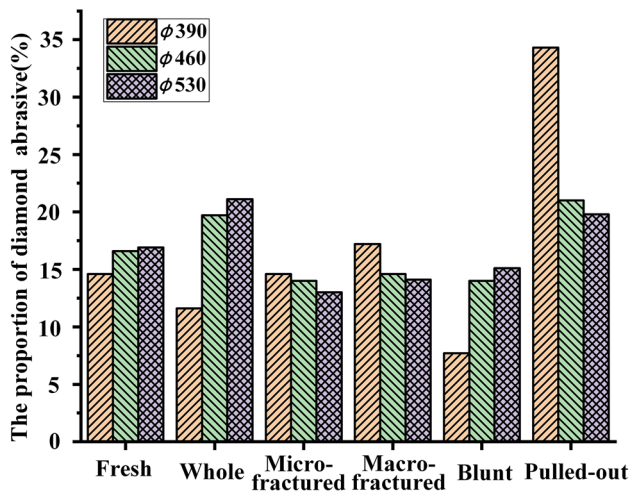
Fig. 12 The failure proportions of worn diamond in segment used by saw blades with different diameters

thickness in the combination saw. Therefore, the rock surface cut by the segment with high linear velocity produced a small and shallow valley. In contrast, the rock surface cut by the segment with a low linear velocity produced a large and deep valley, causing the difference of dissociation and fragmentation of minerals in rocks and differences in the surface roughness of the rock. Furthermore, the maximum undeformed chip shape of diamond particles is transformed from short and thick type to fine and long type, transforming of the removal mechanism of rock from large fragmentation to small fragmentation.

This phenomenon further confirms the conclusion that the maximum undeformed chip thickness per abrasive decreases with increasing diameter of the single saw in the combination saw. From the perspective of being beneficial to the disintegration and removal of granite, the larger chip thickness is beneficial to the material removal of granite; however, it also leads to macro-fractured and pulled-out crystals.
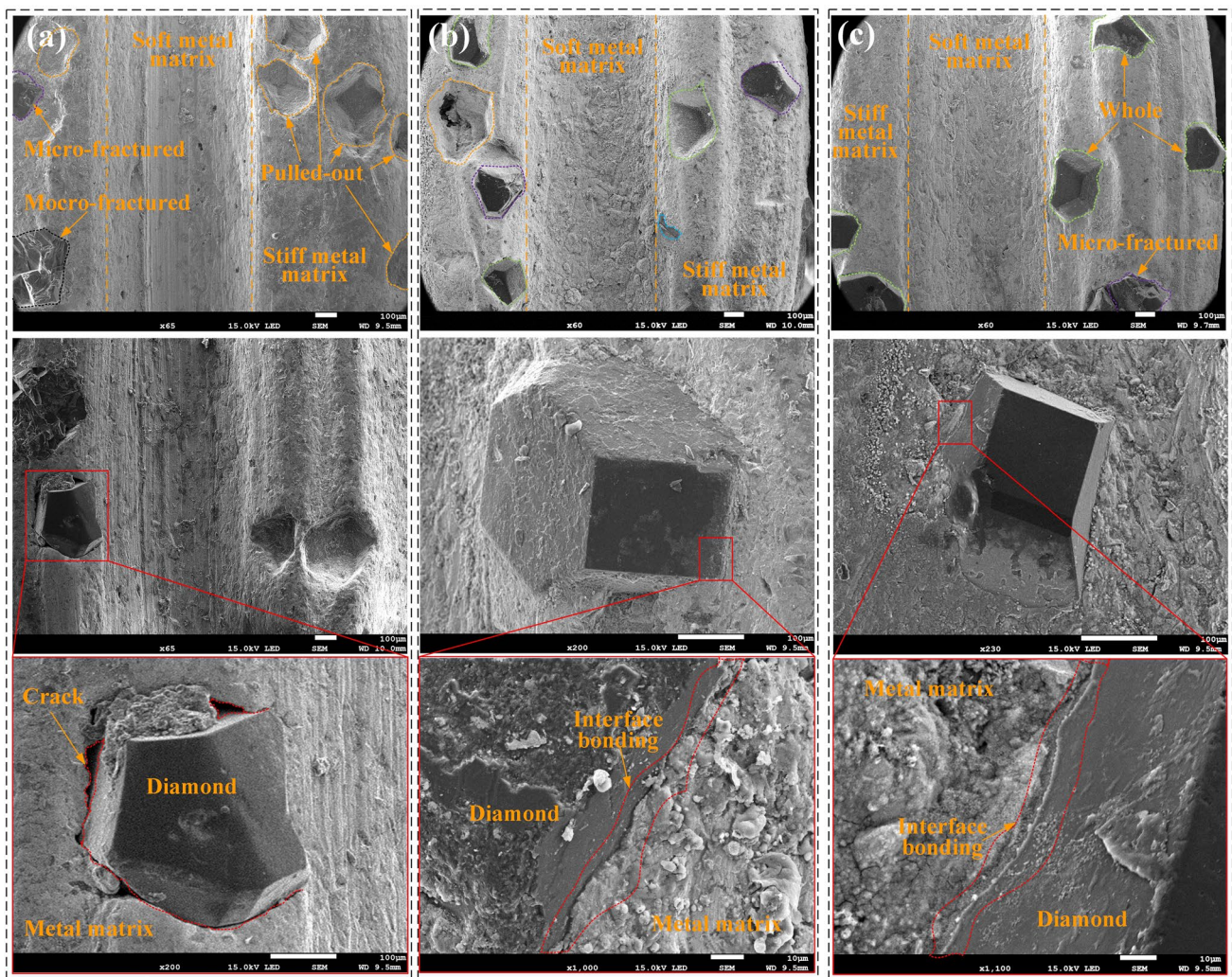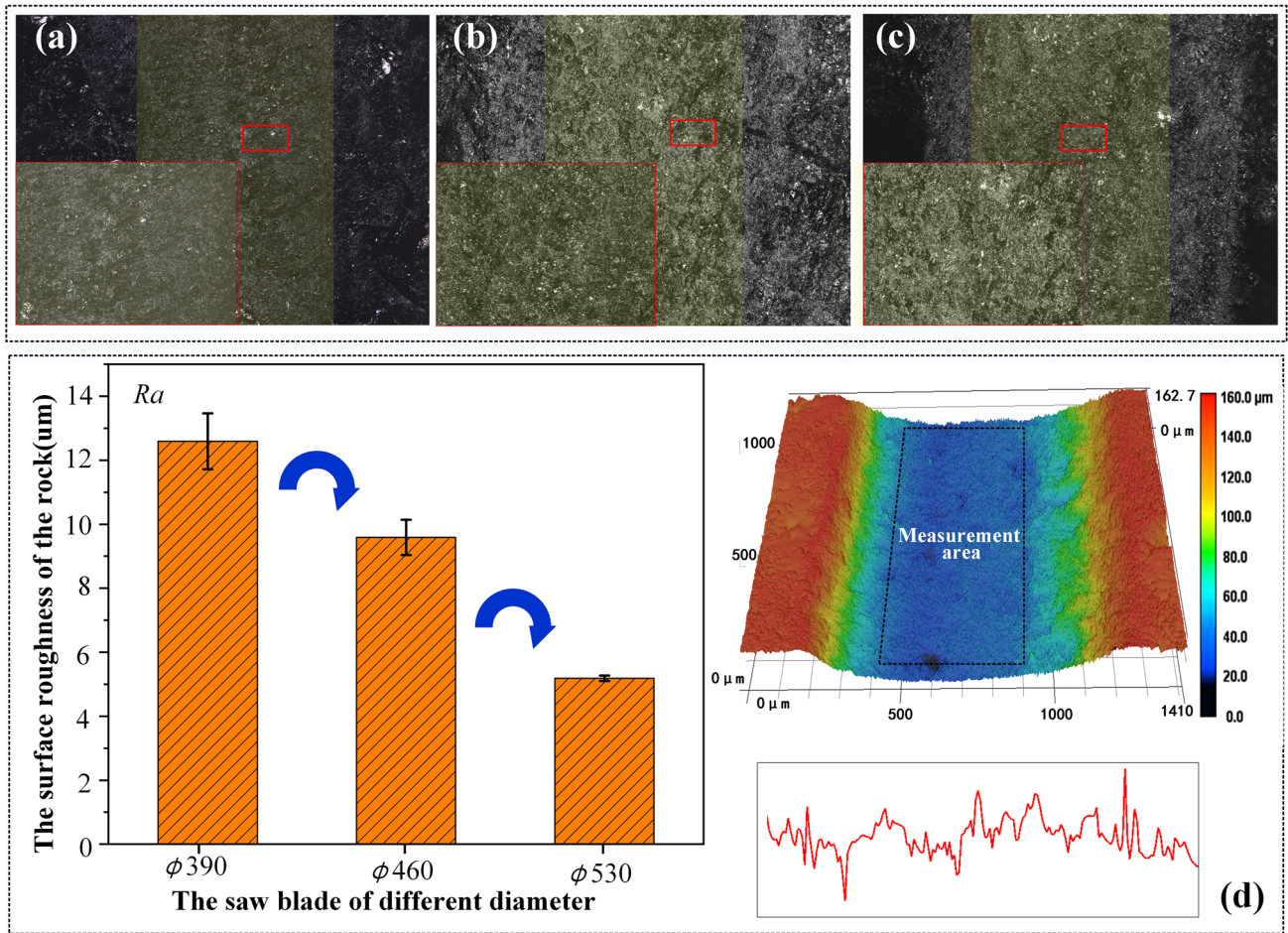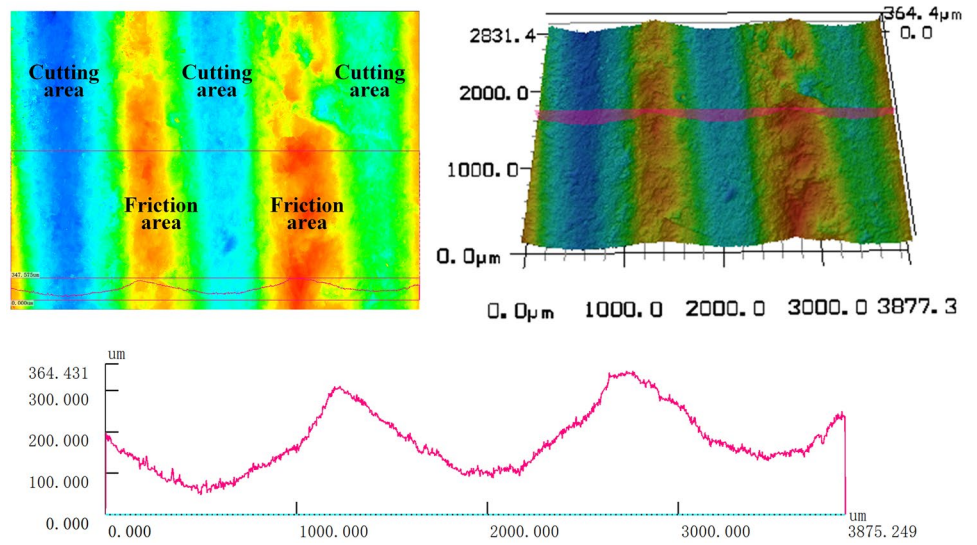

Fig.13 Surface topography of the worn segment on combination saw, **a** φ390, **b** φ460, and **c** φ530

Fig. 14 The rugged sawing trail of the processed rock

Fig. 15 Surface topography and roughness of the rock, **a** surface topography of φ390, **b** surface topographyφ460, **c** surface topography of φ530, and **d** surface roughness of the rock

Therefore, the optimal maximum chip thickness of particles in the appropriate diameter allocations is conducive to the realization of high-efficiency removal of granite.

5 Conclusion

A series of experiments and tests were successfully carried out to investigate the sawing performance of a multidiameter combination saw in granite sawing. The sawing force of the saw blade with different diameters, wear of segments used in the saw blade with different diameters and the sawing trails of rock processed by the saw blade with different diameters were analyzed and compared to provide a direction for optimizing the sawing performance. The main conclusions of this study are as follows:

1. With increasing diameter of the single saw in the combination saw, the maximum undeformed chip thickness and the load per diamond, and the load in the sawing arc zone all decrease. The maximum undeformed chip shape of diamond particles is transformed from short and thick type to thin and long type. The sawing force for the single saw and combination saw increases with increasing feed speed and the sawing depth. The sum of the sawing force of the single saw is generally less than that of the combination saw under the same sawing parameters, indicating a coupling effect between the single saws that affects decomposition and generation of forces in the multidiameter saw.

2. Different failure mechanisms of particles in the worn segment of the tool with different diameters operate in rock processing using a multidiameter combination saw. Because of the negative correlation between the load per diamond and the diameter of the saw blade, the load nonuniformity of diamond appears on the saw blades of different diameters, transforming the grains from abnormal failure to normal cutting. The experiments show the proportion of the whole and blunt diamond particles increases (from 11.6% to 21.15% and 7.7% to 15.1%, respectively) and that the macro-fractured and pulled-out crystals decreases (from 17.2% to 14.1%, and 34.3–19.8%, respectively), providing a guidance for the performance improvements of the multidiameter combination saw, using the different segments (the variation of the metal binder with strong retention capacity and high-quality diamonds) for saw blades of different diameters.

3. The differences in the surface integrity are attributed to the variation in the maximum undeformed chip thickness per abrasive on the saw blade with different diameters in the combination saw. Brittle failure appears as the dominant removal mechanism of rock.

Because of the negative correlation between the maximum undeformed chip thickness and the tool's diameter, the gully depth on the surface of the processed rock and the surface roughness of rock decreases with increasing diameter, and the rock surface eventually tends to flatten out.

This study also directs to explore the effect of changing segments of saw blade in multidiameter saw on rock breakage and tools performance to improve the removal efficiency of rock, in particular, the variations in the structure or quantity of segments. For instance, a reasonable number of segments should be designed on different diameters of saw blades in the multidiameter saw.

Declarations

Conflict of Interest The authors declare that they have no known competing financial interests or personal relationships that could have appeared to influence the work reported in this paper.

References

Aydin G, Karakurt I, Aydiner K (2013a) Development of predictive models for the specific energy of circular diamond sawblades in the sawing of granitic rocks. Rock Mech Rock Eng 46(4):767–783. https://doi.org/10.1007/s00603-012-0290-6

Aydin G, Karakurt I, Aydiner K (2013b) Wear performance of saw blades in processing of granitic rocks and development of models for wear estimation. Rock Mech Rock Eng 46(6):1559–1575. https://doi.org/10.1007/s00603-013-0382-y

Aydin G, Karakurt I, Aydiner K (2013c) Investigation of the surface roughness of rocks sawn by diamond sawblades. Int J Rock Mech Min Sci 61:171–182. https://doi.org/10.1016/j.ijrmms.2013.03.002

Aydin G, Karakurt I, Hamzacebi C (2015) Performance prediction of diamond sawblades using artificial neural network and regression Analysis. Arab J Sci Eng 40(7):2003–2012. https://doi.org/10.1007/s13369-015-1589-x

Bai S, Elwert T, Jia S, Wang Q, Liu T, Yao R (2020) Methodologies for evaluating sawability of ornamental granite and relation modeling combining sawability with environmental impacts: an application in a stone industrial park of China. J Clean Prod 246:119004. https://doi.org/10.1016/j.jclepro.2019.119004

Bayram F, Yasitli N (2013) Effects of sawing parameters on natural stone processing performance. Proc IMechE Part e: J Process Mech Eng 227(4):287–294. https://doi.org/10.1177/0954408912465045

Bayram F, Kulaksiz S (2021) Evaluation of rock cutting performance of diamond segmented frame saw in terms of diamond segment

wear. Int J Rock Mech Min Sci 139:104657. https://doi.org/10.1016/j.ijrmms.2021.104657

Bulut B, Baydogan M, Kayali E (2021) Effect of aluminium and silver addition on the wear characteristics of circular diamond saw blades for cutting ankara andesite rocks. Wear 474–475:203867. https://doi.org/10.1016/j.wear.2021.203867

Buyuksagis I, Rostami J, Yagiz S (2020) Development of models for estimating specific energy and specific wear rate of circular diamond saw blades based on properties of carbonate rocks. Int J Rock Mech Min Sci 135:104497. https://doi.org/10.1016/j.ijrmms.2020.104497

Celep O, Aydin G, Karakurt I (2013) Diamond recovery from waste sawblades: a preliminary investigation. Proc IMechE Part b: J Eng Manuf 227(6):917–921. https://doi.org/10.1177/0954405412471524

Goktan R, Gunes Y (2017) Diamond tool specific wear rate assessment in granite machining by means of knoop micro-hardness and process parameters. Rock Mech Rock Eng 50(9):2327–2343. https://doi.org/10.1007/s00603-017-1240-0

Gupta R (2018) Cutting tool for marble & granite: a review. Int Conference on Mechanical 377:12126

Güneş Yılmaz N (2011) Abrasivity assessment of granitic building stones in relation to diamond tool wear rate using mineralogybased rock hardness indexes. Rock Mech Rock Eng 44:725–733. https://doi.org/10.1007/s00603-011-0166-1

Huang G, Zhang M, Huang H, Guo H, Xu X (2017) Estimation of power consumption in the circular sawing of stone based on tangential force distribution. Rock Mech Rock Eng 51(4):1249–1261. https://doi.org/10.1007/s00603-017-1380-2

Inal S, Erkan I, Aydiner K (2019) Determination of the wear performance of diamond saw blades using inductively coupled plasma. Sadhana 44(5):127. https://doi.org/10.1007/s12046-019-1080-6

Karakurt I, Aydin G, Aydiner K (2013a) Experimental and statistical analysis of cutting force acting on diamond sawblade in sawing of granitic rocks. Proc IMechE Part b: J Eng Manuf 227:286–300. https://doi.org/10.1177/0954405412460971

Karakurt I, Aydin G, Aydiner K (2013b) Predictive modeling of noise level generated during sawing of rocks by circular diamond sawblades. Sadhana 38(3):491–511. https://doi.org/10.1007/s12046-013-0117-5

Kansteiner M, Biermann D (2019) Influence of the diamond grain shape and orientation on the process forces and the mechanical work in scratch tests on basalt stone. Diam Relat Mater 94:65–72. https://doi.org/10.1016/j.diamond.2019.02.027

Luo S (1996) Characteristics of diamond sawblade wear in sawing. Int J Mach Tools Manuf 36(6):661–672. https://doi.org/10.1016/0890-6955(95)00071-2

Macerol N, Franca L, Krajnik P (2020) Effect of the grit shape on the performance of vitrified-bonded CBN grinding wheel. J Mater Process Tech 277:116453. https://doi.org/10.1016/j.jmatprotec.2019.116453

Pellegrin D, Corbin N, Baldoni G, Torrance A (2009) Diamond particle shape: its measurement and influence in abrasive wear. Tribol Int 42(1):160–168. https://doi.org/10.1016/j.triboint.2008.04.007

Polini W, Turchetta S (2004a) Force and specific energy in stone cutting by diamond mill. Int J Mach Tool Manu 44(11):1189–1196. https://doi.org/10.1016/j.ijmachtools.2004.04.001

Polini W, Turchetta S (2004b) Test protocol for micro-geometric wear of sintered diamond tools. Wear 257(3–4):246–256. https://doi.org/10.1016/j.wear.2003.12.008

Polini W, Turchetta S (2005) Evaluation of diamond tool wear. Int J Adv Manuf Technol 26(9–10):959–964. https://doi.org/10.1007/s00170-004-2091-x

Rajpurohit S, Sinha R, Sen P (2020a) Influence of Cerchar hardness index of hard rock granite on wear of diamond tools. Mater

Today: Proceedings 33:5471–5475. https://doi.org/10.1007/s12517-020-06139-3

Rajpurohit S, Sinha R, Sen P (2020b) Effect of the rock properties on sawability of granite using diamond wire saw in natural stone quarries. Arab J Geosci 13:1117. https://doi.org/10.1007/s12517-020-06139-3

Soltani H, Tayebi M (2020) Determination of wear parameters and mechanisms of diamond/copper tools in marble stones cutting. Int J Refract Metals Hard Mater 87:105172. https://doi.org/10.1016/j.ijrmhm.2019.105172

Sun Q, Zhang J, Zhang H, Dong P (2017) Force and segment wear in various granites cutting by diamond frame saw. Proc IMechE Part c: J Mech Eng Sci 232(20):3696–3707. https://doi.org/10.1177/0954406217742937

Tumac D (2015) Predicting the performance of large diameter circular saws based on Schmidt hammer and other properties for some Turkish carbonate rocks. Int J Rock Mech Min Sci 75: 159–168. https://doi.org/10.1016/j.ijrmms.2015.01.015

Turchetta S (2012) Cutting force and diamond tool wear in stone machining. Int J Adv Manuf Technol 61(5–8):441–448. https://doi.org/10.1007/s00170-011-3717-4

Turchetta S, Sorrentino L, Bellini C (2017) A method to optimize the diamond wire cutting process. Diam Relat Mater 71:90–97. https://doi.org/10.1016/j.diamond.2016.11.016

Turchetta S, Sorrentino L (2019) Forces and wear in high-speed machining of granite by circular sawing. Diam Relat Mater 100:107579. https://doi.org/10.1016/j.diamond.2019.107579

Tönshoff H, Denkena B, Apmann H, Asche J (2002) Diamond tools in stone and civil engineering industry: cutting principles, wear and applications. Diam Relat Mate 11(3–6):736–741. https://doi.org/10.1016/S0925-9635(01)00561-1

Ucun I, Aslantas K, Buyuksagis I, Tasgetiren S (2013) Effect of cooling liquids on cutting process using diamond segmented disc of natural stones. Proc IMechE Part c: J Mech Eng Sci 227(10):2315–2327. https://doi.org/10.1177/0954406212473555

Wang F, Liu S, Guo Z, Cao L (2020a) Analysis of cutting forces and chip formation in milling of marble. Int J Adv Manuf Technol 108(2):2907–2916. https://doi.org/10.1007/s00170-020-05575-5

Wang F, Liu S, Ji K (2020b) Numerical study on abrasive machining of rock using FDEM method. Simul Model Practi Th 104:102145. https://doi.org/10.1016/j.simpat.2020.102145

Xu X, Li Y, Yu Y (2003) Force ratio in the circular sawing of granites with a diamond segmented blade. J Mater Process Tech 139(1):281–285. https://doi.org/10.1016/S0924-0136(03)00236-X

Yurdakul M (2015) Effect of cutting parameters on consumed power in industrial granite cutting processes performed with the multi-disc block cutter. Int J Rock Mech Min Sci 76:104–111. https://doi.org/10.1016/j.ijrmms.2015.03.008

Zhang H, Zhang J, Wang Z, Sun Q, Fang J (2016) A new frame saw machine by diamond segmented blade for cutting granite. Diam Relat Mater 69:40–48. https://doi.org/10.1016/j.diamond.2016.07.003

Zhang H, Zhang J, Wang S (2019) Comparison of wear performance of diamond tools in frame sawing with different trajectories. Int J Refract Metals Hard Mater 78:178–185. https://doi.org/10.1016/j.ijrmhm.2018.09.012

Zhou J, Zhang J, Zhou H, Dong P, Wang K (2021) Wear characteristics of diamond segments on multi-blade combination saw with different diameters in granite sawing. Int J Refract Metals Hard Mater 97:105517. https://doi.org/10.1016/j.ijrmhm.2021.105517